

# HKAN: Hierarchical Kolmogorov-Arnold Network without Backpropagation

Grzegorz Dudek, Tomasz Rodak

**Abstract**—This paper introduces the Hierarchical Kolmogorov-Arnold Network (HKAN), a novel network architecture that offers a competitive alternative to the recently proposed Kolmogorov-Arnold Network (KAN). Unlike KAN, which relies on backpropagation, HKAN adopts a randomized learning approach, where the parameters of its basis functions are fixed, and linear aggregations are optimized using least-squares regression. HKAN utilizes a hierarchical multi-stacking framework, with each layer refining the predictions from the previous one by solving a series of linear regression problems. This non-iterative training method simplifies computation and eliminates sensitivity to local minima in the loss function. Empirical results show that HKAN delivers comparable, if not superior, accuracy and stability relative to KAN across various regression tasks, while also providing insights into variable importance. The proposed approach seamlessly integrates theoretical insights with practical applications, presenting a robust and efficient alternative for neural network modeling.

**Index Terms**—Kolmogorov-Arnold network, neural networks, multi-stacking, randomized learning.

## I. INTRODUCTION

KOLMOGOROV-ARNOLD Networks (KANs), introduced in [1], represent a paradigm shift in neural network (NN) architecture, offering a promising alternative to traditional Multi-Layer Perceptrons (MLPs). Rooted in the Kolmogorov-Arnold representation theorem, which states that any multivariate continuous function  $f : [0, 1]^n \rightarrow \mathbb{R}$  can be represented as a superposition of continuous functions of a single variable and the binary operation of addition, KANs fundamentally reimagine the structure of NNs.

KANs introduce a significant architectural innovation: unlike MLPs with fixed activation functions on nodes, KANs employ learnable activation functions on edges. Notably, KANs eliminate linear weights entirely, replacing each weight parameter with a univariate function parametrized as a spline. This seemingly simple modification yields significant improvements in both accuracy and interpretability. In terms of accuracy, smaller KAN models consistently achieve comparable or superior performance to larger MLPs in data fitting and partial differential equations solving tasks. Both theoretical analysis and empirical evidence suggest that KANs exhibit faster neural scaling laws than MLPs. Regarding interpretability, KANs

G. Dudek is with (i) the Faculty of Electrical Engineering, Czestochowa University of Technology, (ii) the Faculty of Mathematics and Computer Science, University of Lodz, and (iii) the Centre for Data Analysis, Modelling and Computational Sciences (CAMINO), University of Lodz, e-mail: grzegorz.dudek@pcz.pl.

T. Rodak is with the Faculty of Mathematics and Computer Science, University of Lodz, e-mail: tomasz.rodak@wmii.uni.lodz.pl.

offer intuitive visualization and facilitate easy interaction with human users, enhancing their potential as collaborative tools for scientific discovery.

The unique properties of KANs make them valuable collaborators in helping scientists discover mathematical and physical laws, bridging the gap between machine learning and traditional scientific inquiry. As promising alternatives to MLPs, KANs open new avenues for improving contemporary deep learning models, which heavily rely on MLP architectures.

## A. Related Work

Recent research has highlighted the potential of KANs as efficient and interpretable alternatives to traditional MLPs [2]–[4]. Unlike MLPs, KANs replace linear weights with learnable activation functions, enabling dynamic pattern learning and improved performance with fewer parameters. Studies have shown that KANs can achieve comparable or even superior accuracy to larger MLPs, faster neural scaling laws, and enhanced interpretability [5]. From a theoretical perspective, Wang et al. [6] demonstrated that the approximation and representation capabilities of KANs are at least equivalent to those of MLPs. Furthermore, KAN’s multi-level learning approach, particularly its grid extension of splines, enhances the modeling of high-frequency components. While MLPs often suffer from catastrophic forgetting, collaborative filtering-based KANs have been proposed to address this issue [7].

Despite these advancements, KANs are not without criticism. Some studies argue that KAN outperforms MLPs primarily in symbolic formula representation but falls short in tasks like computer vision, natural language processing, and audio processing [8]. Tran et al. [9] reported that despite their theoretical advantages, KANs do not consistently outperform MLPs in practical classification tasks. Additionally, their hardware implementations tend to be less efficient, with higher resource usage and latency. Sensitivity to noise is another limitation; even minimal noise in the data can significantly degrade performance [10].

To enhance the interpretability, interactivity, and versatility of KAN, Liu et al. [11] introduced MultKAN, which incorporates multiplication operations. By integrating multiplication nodes, MultKAN explicitly represents multiplicative structures, allowing for a more transparent mapping of physical laws and improved modeling of complex relationships.

KANs have also been integrated with other architectures to address diverse challenges. In computer vision, [12] combined KAN with convolutional layers, demonstrating that KAN

convolutions maintain similar accuracy while using half the parameters. Residual KANs, introduced in [13], effectively capture long-range, nonlinear dependencies within CNNs by incorporating KAN as a residual component.

Genet and Inzirillo [14] proposed integrating KANs with transformers to simplify complex dependencies in time series while enhancing interpretability. Temporal KANs, combining KAN with LSTMs, were introduced in [15] for multi-step time series forecasting. These networks integrate memory management through recurrent KAN layers. Subsequent work by the same authors refined this approach by incorporating transformers and learnable path signatures to capture geometric features [16].

Yang and Wang [17] introduced the Kolmogorov-Arnold transformer, replacing MLP layers with KAN layers to improve model expressiveness and performance. In graph NNs networks, [18] replaced MLPs with KANs for feature extraction, resulting in the GraphKAN architecture. Li et al. [19] tailored a KAN-GNN model for molecular representation learning, emphasizing KAN's flexibility in diverse domains.

KANs have also been employed in evolutionary algorithms as surrogate models for regression and classification tasks [20], helping to reduce the number of expensive function evaluations during optimization. Additionally, [21] introduced probabilistic KANs by incorporating Gaussian process neurons, enabling robust nonlinear modeling with uncertainty estimation.

The flexibility of KANs has led to explorations with various activation functions beyond B-splines, including wavelets [22], radial basis functions [23], Fourier series [24], Jacobi basis functions [25], rational functions [26], and ReLU [27]. A comprehensive comparison of activation functions used in KAN architectures is available in [28].

Numerous enhancements have been proposed for KANs, such as dropout-based regularization [29], adaptive grid updates [30], federated learning [31], and reinforcement learning [32]. These advancements, combined with KAN's interpretability and flexibility, have enabled its application across a wide range of fields, including tabular data [33], computer vision [12], [34], graphs [18], time series [15], [35]–[37], recommender systems [7], neuroscience [38], quantum science [39], biology [40], and survival analysis [41].

### B. Motivation and Contributions

KAN models are traditionally trained using backpropagation algorithms, which rely on gradients of the network's loss function with respect to its parameters. However, gradient-based learning processes are sensitive to issues such as local minima, flat regions, and saddle points in the loss function. Additionally, gradient calculations can be computationally expensive, particularly for deep and wide network architectures, complex target functions, and large training datasets.

In this study, we propose a randomized learning approach for training KANs as an alternative to backpropagation. Unlike gradient-based methods, which lead to non-convex optimization problems, the randomized approach transforms the problem into a convex one [42]. This is achieved by fixing the parameters of the activation functions, which are selected

either randomly or based on the data, and remain unchanged during training. The only adaptation occurs in the linear functions that aggregate the outputs of the basis functions and activation functions. Since the optimization problem becomes linear, the model's weights can be efficiently learned using a standard least-squares method. This significantly simplifies the training process and accelerates computation compared to gradient-based approaches. Numerous studies in the literature have demonstrated the high performance of randomized neural models compared to fully trainable ones [43]–[50].

Our approach begins with utilizing fixed parameters for basis functions, determined either by data or randomly. These basis functions are then combined in multiple blocks using linear regression. The resulting block functions (activation functions) are subsequently combined through linear regression, and this iterative process is repeated across subsequent layers to form higher-level representations. Combining diverse blocks corresponds to ensembling, while performing it layer by layer constitutes a multi-stacking approach. This hierarchical modeling of the target function progressively enhances accuracy at each level, eliminating the need for backpropagation.

Our study makes three significant contributions to the field of NNs, specifically in the domain of KANs:

- 1) Novel Training Method for KAN: We introduce an innovative approach to training KANs that eliminates the need for backpropagation. The parameters of basis functions are fixed, determined either randomly or based on data. The model is trained hierarchically using the standard least-squares method. This approach results in a more efficient and robust training process for KANs, offering improvements in both computational efficiency and model accuracy.
- 2) Multi-Stacking Approach for Prediction: Our hierarchical KAN (HKAN) implements hierarchically multi-stacking approach to built predictions. In each layer, meta-learners combine predictions performed by weak learners (univariate models). Subsequent layers, fed by predictions from previous layers, successively refine the results, enhancing overall accuracy layer by layer.
- 3) Empirical Results for Regression Problems: We provide comprehensive empirical evidence demonstrating that our HKAN outperforms standard KAN in a range of regression problems.

The remainder of this paper is organized as follows: Section II provides an overview of the Kolmogorov-Arnold representation theorem and standard KANs, establishing the foundation for our research. Section III introduces the proposed HKAN model, detailing its architecture, components, features, and learning process. Section IV presents a comparison between HKAN and KAN, while Section V examines HKAN through the lens of multi-stacking models. The experimental framework used to evaluate the proposed model is described in Section VI. Finally, Section VII concludes the paper.

## II. PRELIMINARY

### A. Kolmogorov-Arnold Representation Theorem

The Kolmogorov–Arnold representation theorem, also known as the superposition theorem, stands as a cornerstone

in the theory of function approximation. This profound result asserts that any continuous function of several variables can be represented as a composition of continuous functions of one variable and addition.

For any continuous function  $f : [0, 1]^n \rightarrow \mathbb{R}$ , there exist continuous functions  $\phi_{q,p} : [0, 1] \rightarrow \mathbb{R}$  and  $\Phi_q : \mathbb{R} \rightarrow \mathbb{R}$  such that:

$$f(x_1, \dots, x_n) = \sum_{q=1}^{2n+1} \Phi_q \left( \sum_{p=1}^n \phi_{q,p}(x_p) \right) \quad (1)$$

The theorem carries significant implications for function approximation and theoretical computer science. It suggests a universal approximation capability, implying that any multivariate continuous function can be approximated by a network of simple, single-variable functions. Notably, the outer functions  $\Phi_q$  are independent of the function  $f$  being approximated, serving as universal building blocks. This property effectively reduces the problem of approximating  $n$ -dimensional functions to that of approximating one-dimensional functions.

However, the theorem's practical application faces certain limitations. The inner functions  $\phi_{q,p}$  can be highly non-smooth, even when  $f$  is smooth, potentially complicating computational implementation. Moreover, while theoretically powerful, the representation may not be efficiently computable in practice.

The Kolmogorov–Arnold representation theorem stands as a bridge between pure mathematics and applied computational science, highlighting the potential for representing complex functions through simpler components while also illustrating the challenges in translating theoretical results into practical applications.

### B. Kolmogorov–Arnold Networks (KANs)

Paper [1] extends and modifies the Kolmogorov–Arnold representation theorem to create Kolmogorov–Arnold Networks (KANs) in several key ways. While the original theorem uses a 2-layer network with a specific width in the hidden layer, KANs generalize this to allow arbitrary widths and depths, stacking multiple "KAN layers".

A KAN layer is defined as a matrix of activation functions  $\phi_{q,p}$ , where  $q$  is not restricted to the theoretical limit of  $2n+1$ :

$$\phi(\mathbf{x}) = \begin{bmatrix} \phi_{1,1}(x_1) & \dots & \phi_{1,n_{in}}(x_{n_{in}}) \\ \vdots & \ddots & \vdots \\ \phi_{n_{out},1}(x_1) & \dots & \phi_{n_{out},n_{in}}(x_{n_{in}}) \end{bmatrix} \quad (2)$$

where  $x_p$  denotes the  $p$ -th input to the layer,  $n_{in}$  denotes the number of inputs, and  $n_{out}$  denotes the number of outputs (not restricted to  $2n+1$ ).

Deeper KANs are created by composing multiple KAN layers. Unlike the original theorem which allows non-smooth or even fractal functions, KANs assume smooth activation functions to facilitate learning. The authors propose activation functions parameterized as B-splines with trainable coefficients combined with the sigmoid linear unit (SiLU). Note the substantial difference between KANs and MLPs: instead of fixed multidimensional activation functions on nodes as

TABLE I: List of the Main Symbols.

Symbol	Meaning
BaF	basis function
BIF	block function (activation function)
$n$	number of inputs
$N$	number of training samples
$\mathbf{x} \in [0, 1]^n$	input pattern
$\mathbf{z}^{(l)} \in \mathbb{R}^{n^{(l)}}$	output vector of layer $l$ and input vector to layer $l + 1$
$y \in [0, 1]$	target
$\hat{y} \in \mathbb{R}$	prediction
$l, L$	layer index and the total number of layers, respectively
$n^{(l)}$	width of the $l$ -th layer (number of nodes)
$m^{(l)}$	number of BaFs in a block of layer $l$
$p$	input index to layer $l$ , $p = 1, \dots, n^{(l-1)}$
$q$	output index of layer $l$ , $q = 1, \dots, n^{(l)}$
$r$	BaF index in a block in layer $l$ , $r = 1, \dots, m^{(l)}$
$g_{q,p,r}^{(l)}$	BaF in layer $l$
$\phi_{q,p}^{(l)}$	BIF in layer $l$ , i.e. linear combination of $g_{q,p,r}^{(l)}$
$h_q^{(l)}$	$q$ -th output of layer $l$ , i.e. linear combination of $\phi_{q,p}^{(l)}$
$c_{q,p,r}^{(l)}$	weight of BaF $g_{q,p,r}^{(l)}$
$w_{q,p}^{(l)}$	weight of BIF $\phi_{q,p}^{(l)}$
$\mu_{q,p,r}^{(l)}$	location parameter of BaF $g_{q,p,r}^{(l)}$
$\sigma^{(l)}$	smoothing parameter in layer $l$
$\lambda_\phi^{(l)}, \lambda_h^{(l)}$	regularization parameters for functions $\phi$ and $h$ in layer $l$

in MLPs, KANs use learnable one-dimensional activation functions on edges.

The paper introduces a grid extension technique, allowing KANs to be made more accurate by refining the spline grids of the activation functions. This enables increasing model capacity without retraining from scratch.

The authors also introduce sparsification and pruning techniques to simplify KANs and discover minimal architectures that match the data structure. New theoretical guarantees are provided for KANs with finite grid sizes, suggesting that they can beat the curse of dimensionality for functions with compositional structure.

Furthermore, the paper provides tools for users to visualize and modify KANs, making them more interpretable and interactive. This approach takes the core idea of representing multivariate functions using univariate functions and addition, and extends it into a flexible, trainable NN architecture with theoretical guarantees and practical advantages over standard MLPs. In essence, [1] modernizes the Kolmogorov–Arnold theory for use in contemporary machine learning, offering a new perspective on function approximation and NN design.

### III. HIERARCHICAL KAN

Table I provides a summary of the main symbols used throughout this study for clarity and reference. The implementation of the proposed model is available in our GitHub repository [51].

#### A. Architecture

HKAN is an advanced NN architecture inspired by the Kolmogorov–Arnold representation theorem. While it shares similarities with the KAN architecture, HKAN introduces unique components and a distinct training process. The architecture of HKAN is shown in Fig. 1.

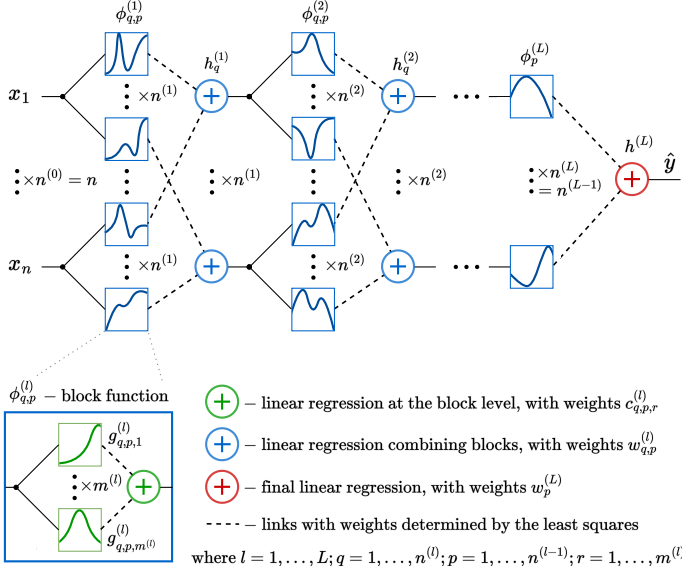


Fig. 1: HKAN architecture.

Let  $\mathbf{z}^{(l-1)}$  be the input vector for layer  $l$ . The first layer of HKAN takes input vector  $\mathbf{z}^{(0)} = \mathbf{x} = [x_1, \dots, x_n]^\top \in \mathbb{R}^n$ . Each component of the input vector is transformed by a group of blocks. Within each group, there are  $n^{(l)}$  blocks, and each block projects its input nonlinearly using  $m^{(l)}$  basis functions (BaFs). Consider two common basis functions: Gaussian

$$g(z) = \exp\left(-(\sigma(z - \mu))^2\right) \quad (3)$$

and sigmoid

$$g(z) = \frac{1}{1 + \exp(-\sigma(z - \mu))} \quad (4)$$

where  $\mu$  is the location parameter, and  $\sigma$  is the smoothing parameter corresponding to the slope or bandwidth of the BaF.

The configuration of BaFs plays a crucial role in the network's performance. The number of BaFs, together with the smoothing parameter, serve as hyperparameters that define the block's flexibility and balance the trade-off between variance and bias in the output. The locations of the BaFs, denoted as  $\mu_{q,p,r}^{(l)}$  for the  $r$ -th function in the block corresponding to  $\phi_{q,p}^{(l)}$ , define the position of the maximum for Gaussian functions or the inflection point for sigmoid functions. To distribute BaFs in a block across the input interval (typically a bounded region of  $[0, 1]$ ), these locations can be selected in two ways:

- Random uniform distribution: The locations are drawn from a uniform distribution,  $\mu_{q,p,r}^{(l)} \sim U(0, 1)$ , ensuring random spread across the input range.
- Data-driven distribution (support point method): In this approach, locations are assigned to randomly selected training points (in the first layer) or their projections (in subsequent layers), called support points:  $\mu_{q,p,r}^{(l)} = z_{\xi,p}^{(l-1)}$ , where  $\xi \sim U\{1, \dots, N\}$ .

The support point method aligns the BaFs with the data distribution, avoiding empty regions in the input space (see Fig. 2).

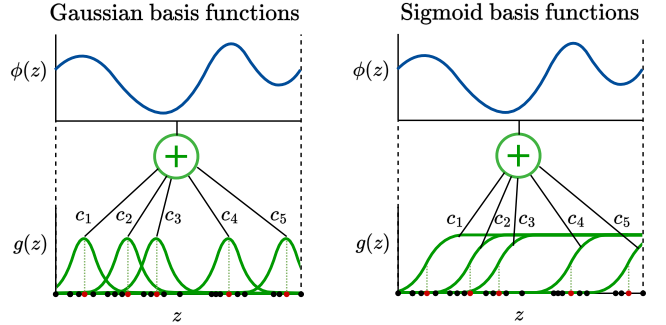


Fig. 2: Illustration of block function composition using the support point method. Red markers represent the support points that determine the placement of BaFs.

The BaFs within a block,  $g_{q,p,r}^{(l)} : \mathbb{R} \rightarrow \mathbb{R}$ , are combined using linear regression:

$$\phi_{q,p}^{(l)}(z_p^{(l-1)}) = \sum_{r=1}^{m^{(l)}} c_{q,p,r}^{(l)} g_{q,p,r}^{(l)}(z_p^{(l-1)}) \quad (5)$$

Resulting function  $\phi_{q,p}^{(l)} : \mathbb{R}^{m^{(l)}} \rightarrow \mathbb{R}$  is called a block function (BIF). The weights of each BIF,  $c_{q,p,r}^{(l)}$ , are determined using least squares by minimizing the sum of squared residuals:

$$L = \sum_{i=1}^N (y_i - \hat{y}_i)^2 \quad (6)$$

where  $\hat{y}_i$  is a prediction performed by the BIF:  $\hat{y}_i = \phi_{q,p}^{(l)}(z_{i,p}^{(l-1)})$ .

The weights of  $\phi_{q,p}^{(l)}$  can be calculated analytically as

$$\mathbf{c}_{q,p}^{(l)} = \mathbf{G}_{q,p}^{(l)+} \mathbf{y} \quad (7)$$

where  $\mathbf{c}_{q,p}^{(l)} = [c_{q,p,1}^{(l)}, \dots, c_{q,p,m^{(l)}}^{(l)}]^\top$ ,  $\mathbf{y} = [y_1, \dots, y_N]^\top$  and  $\mathbf{G}_{q,p}^{(l)+}$  is the Moore–Penrose generalized inverse of the BaF response matrix to the  $N$  training data points or their projections:

$$\mathbf{G}_{q,p}^{(l)} = \begin{bmatrix} g_{q,p,1}(z_{p,1}^{(l-1)}) & \dots & g_{q,p,m^{(l)}}(z_{p,1}^{(l-1)}) \\ \vdots & \ddots & \vdots \\ g_{q,p,1}(z_{p,N}^{(l-1)}) & \dots & g_{q,p,m^{(l)}}(z_{p,N}^{(l-1)}) \end{bmatrix} \quad (8)$$

For the  $p$ -th input, each block in a group fits different function (due to random positioning of BaFs) that approximate the target function based on this input. Consequently, there are a total of  $n^{(l-1)} n^{(l)}$  BIFs in layer  $l$ . In the subsequent step, these BIFs are combined linearly by  $n^{(l)}$   $h$ -functions. Each  $q$ -th  $h$ -function takes as input the  $q$ -th BIF from every group. Thus, each  $h$ -function approximates the target function based on different projections of all components of the input pattern for layer  $l$ :

$$h_q^{(l)}(\mathbf{z}^{(l-1)}) = \sum_{p=1}^{n^{(l-1)}} w_{q,p}^{(l)} \phi_{q,p}^{(l)}(z_p^{(l-1)}) \quad (9)$$

The weights of this combination are calculated as:

$$\mathbf{w}_q^{(l)} = \Phi_q^{(l)+} \mathbf{y} \quad (10)$$

where  $\mathbf{w}_q^{(l)} = [w_{q,1}^{(l)}, \dots, w_{q,n^{(l)}}^{(l)}]^\top$ , and  $\Phi_q^{(l)+}$  is the Moore–Penrose generalized inverse of the Blf response matrix to the projections of  $N$  training data points:

$$\Phi_q^{(l)} = \begin{bmatrix} \phi_{q,1}(z_{1,1}^{(l-1)}) & \dots & \phi_{q,n^{(l-1)}}(z_{n^{(l-1)},1}^{(l-1)}) \\ \vdots & \ddots & \vdots \\ \phi_{q,n^{(l)}}(z_{1,N}^{(l-1)}) & \dots & \phi_{q,n^{(l)}}(z_{n^{(l-1)},N}^{(l-1)}) \end{bmatrix} \quad (11)$$

Weights (10) minimize loss function (6), where  $\hat{y}_i$  is a prediction performed by the  $h$ -function:  $\hat{y}_i = h_q^{(l)}(\mathbf{z}_i^{(l-1)})$ .

The output of layer  $l$  is given by  $\mathbf{z}^{(l)} = \hat{\mathbf{y}}^{(l)} = [\hat{y}_1^{(l)}, \dots, \hat{y}_{n^{(l)}}^{(l)}]^\top \in \mathbb{R}^{n^{(l)}}$ , where each component  $\hat{y}_q^{(l)} = h_q^{(l)}(\mathbf{z}^{(l-1)})$ . This output is then fed to the next layer and processed using (5)–(11).

Following the design of the original KAN, the structure of the top layer (layer  $L$ ) in HKAN differs slightly from the preceding layers, as it includes only one BaF per input. The final output of HKAN is obtained through a linear combination of the  $n^{(L)} = n^{(L-1)}$  Blfs:

$$h^{(L)}(\mathbf{z}^{(L-1)}) = \sum_{p=1}^{n^{(L)}} w_p^{(L)} \phi_q^{(L)}(z_p^{(L-1)}) \quad (12)$$

In HKAN, we employ standard linear regression, which is applied multiple times both at the block level (Blfs) and for combining multiple blocks ( $h$ -functions). However, to mitigate overfitting, we can alternatively use regularized least squares (ridge regression). In the experimental part of this work, we adopt this variant to calculate the weights of Blfs,  $\phi_{q,p}^{(l)}$ . The weights in this case are computed using the following closed-form solution:

$$\mathbf{c}_{q,p}^{(l)} = (\mathbf{G}_{q,p}^{(l)\top} \mathbf{G}_{q,p}^{(l)} + \lambda_\phi^{(l)} \mathbf{I})^{-1} \mathbf{G}_{q,p}^{(l)\top} \mathbf{y} \quad (13)$$

where  $\mathbf{I}$  is an identity matrix and  $\lambda_\phi^{(l)} \geq 0$  is a regularization parameter.

## B. Learning

The optimization problem in HKAN is decomposed into multiple linear regression subproblems. Each subproblem minimizes objective function (6) using the least squares method. Since these optimization subproblems are convex, the least squares approach guarantees optimal weights (within the context of the randomly selected BaFs).

The learning process in HKAN is hierarchical. First, the target function is simultaneously approximated by the blocks of the first layer, with each block modeling the target based on a single input variable. Due to the nonlinear nature of the BaFs, this step introduces nonlinearity into the modeling process. Then, based on these approximations, multiple  $h$ -functions are fitted to the target function. Each  $h$ -function linearly combines single-variable Blfs, producing a multivariable mapping.

Subsequent layers transform their inputs in a similar manner, involving three key steps: (1) nonlinear projections of individual inputs by BaFs, (2) linear combinations of BaFs within each block, and (3) linear combinations of Blfs. Each layer refines the predictions generated by the preceding layers, aiming to improve the overall approximation.

It is important to note that BaFs are not learned; their parameters, namely location ( $\mu$ ) and smoothing ( $\sigma$ ), remain fixed. Randomness in  $\mu$  introduces diversity among Blfs. This diversity is advantageous for ensembling, which is carried out by the  $h$ -functions. The benefits of this approach are discussed in greater detail in Section V.

## C. Hyperparameters

The HKAN hyperparameters are as follows:

- $L$  – total number of layers,
- $n^{(l)}$  – width of the  $l$ -th layer (number of nodes),
- $m^{(l)}$  – number of BaFs in blocks of layer  $l$ ,
- BaF type,
- Way to generate location parameters of BaFs ( $\mu$ ),
- $\sigma^{(l)}$  – smoothing parameter in layer  $l$ ,
- $\lambda_\phi^{(l)}, \lambda_h^{(l)}$  – regularization parameters for functions  $\phi$  and  $h$  in layer  $l$  (optional).

Intuitively, a more complex target function needs a deeper and wider network to model it with higher accuracy. The modeling burden can be shifted at the block level. In such a case many BaFs are needed (with  $\sigma$ -parameter adjusted to the approximation problem complexity) and less  $h$ -functions. Opposite situation is also possible: a small number of BaFs roughly approximates the target function, and the effort of a more accurate approximation falls on a large number of  $h$ -functions.

It is important to note that the regression problem solved at each level of HKAN processing can vary. At the initial level, the target function is approximated based directly on input patterns  $\mathbf{x}$ , whereas at subsequent levels, it is approximated based on the predictions generated by the previous level. Consequently, the complexity of the problems addressed at different levels may differ, necessitating distinct values for layer-specific hyperparameters  $n^{(l)}$ ,  $m^{(l)}$ ,  $\sigma^{(l)}$ , and optionally  $\lambda_\phi^{(l)}$  and  $\lambda_h^{(l)}$ .

HKANs with more layers, more nodes, more BaFs and with smaller values of the parameters  $\sigma$  and  $\lambda$  tend to fit the target function more accurately. However, such configurations are more susceptible to overfitting. Therefore, these parameters must be carefully tuned to strike an optimal balance between the model's bias and variance.

The strategy for generating  $\mu$  values, which determine the positions of BaFs, depends on the anticipated data distribution. When the distribution of new, unseen data points is expected to closely mirror that of the training dataset, positioning BaFs at the training points is often an effective approach. This method ensures that the network's approximation capability is concentrated in regions where data is most likely to occur. Conversely, if the distribution of new data is expected to differ from the training set, or if the goal is to create a more generalized model, a random distribution of BaFs may be

preferable. This approach allows for broader coverage of the input space, including regions that may be sparsely represented or entirely absent in the training data.

Determining the optimal shape of BaFs a priori is challenging, as it often depends on the specific characteristics of the target function. In HKAN, different types of BaFs can be mixed flexibly. They may vary across layers, between blocks within the same layer, or even within individual blocks. In such cases, the smoothing parameters should be customized for each type of BaF to ensure optimal performance and adaptability.

#### D. Complexity

In layer  $l$ , each block performs linear regression on  $m^{(l)}$  BaFs with a complexity of  $O(Nm^{(l)2} + m^{(l)3})$ . For layers  $l = 1, \dots, L - 1$ , each containing  $n^{(l-1)}n^{(l)}$  blocks, the total complexity per layer is  $O(n^{(l-1)}n^{(l)}(Nm^{(l)2} + m^{(l)3}))$ . The top layer contains  $n^{(L)}$  blocks, resulting in a complexity of  $O(n^{(L)}(Nm^{(L)2} + m^{(L)3}))$ .

Each function  $h_q^{(l)}$  linearly combines  $n^{(l-1)}$  blocks, yielding a complexity of  $O(Nn^{(l-1)2} + n^{(l-1)3})$ . For layers  $l = 1, \dots, L - 1$ , with  $n^{(l)}$  such functions per layer, the total complexity becomes  $O(n^{(l)}(Nn^{(l-1)2} + n^{(l-1)3}))$ . The final layer produces a single output, resulting in a complexity of  $O(Nn^{(L)2} + n^{(L)3})$ .

## IV. HKAN VS STANDARD KAN

This section outlines the key differences between KAN as defined in [1] and our proposed HKAN.

#### A. Basis Functions

KAN employs B-splines of order 3, which are bell-shaped and computed recursively using the Cox-de Boor formula. The properties of these BaFs, including their number, location, width, and support, are determined by knots. In KANs, these knots are positioned at equidistant intervals, resulting in an even distribution of the basis functions across the input space. The number of knots, which directly influences the spline's flexibility and the model's capacity to capture complex patterns, is a crucial hyperparameter in the KAN architecture.

In contrast, HKANs offer greater flexibility in the selection of BaF types. While in Section III-A we introduced Gaussian and sigmoid functions, the HKAN framework is not limited to these and can accommodate various other functional forms (see experimental part of this work, Section VI). Unlike KANs, the distribution of BaFs in HKANs can be either data-driven or random. In the HKAN framework, the smoothing parameter and the number of BaFs serve as key hyperparameters. The adaptability in both function type and distribution allows HKANs to potentially capture a wider range of functional relationships within the data.

When evaluating computational efficiency, it should be noted that KAN uses B-splines, whose computation involves recursive processes, making it computationally intensive. In contrast, HKAN does not require a recursive process to create BaFs, potentially reducing computational complexity.

#### B. Block Functions (Activation Functions)

In KAN, what we refer to as a BIF is termed an activation function. This activation function is a composite structure, consisting of two main components: a weighted sum of a spline (which itself is a linear combination of BaFs with trainable weights  $c$ ) and a SiLU. The incorporation of SiLU was likely designed to enhance the network's training dynamics. In the KAN architecture, the BIFs are aggregated without additional weighting.

HKAN employ a distinct methodology. In this framework, BIFs are also constructed by combining BaFs with weights  $c$ , similar to KAN. However, unlike in KAN, these weights are not optimized via gradient descent. Instead, they are computed using the least-squares method, with the goal of fitting each BIF to the target function in a one-dimensional space. This method provides a more direct, analytical determination of the weights. The HKAN then linearly combines these BIFs, once again using weights determined through the least-squares method, to approximate the target function in multi-dimensional space.

#### C. Explainability and Function Representation

In KANs, BIFs serve as interpretable building blocks, designed with the flexibility to be replaced by specific symbolic forms such as polynomial, sine, or logarithmic functions. This design philosophy enables transparent construction of complex functions from simpler components, iterative refinement of the target function during the training process, and potential for direct translation into human-readable mathematical expressions. This modular approach facilitates a bottom-up understanding of the learned function, allowing researchers to dissect and analyze the contribution of each component to the overall model behavior.

HKANs, on the other hand, employ BIFs in a fundamentally different manner. Each BIF attempts to approximate the target function within a one-dimensional space. This approach provides a direct measure of individual input variable importance, with the quality of these one-dimensional approximations serving as a metric for assessing the expressive power of each input variable. This characteristic of HKANs allows us to quickly identify key input arguments and gauge their significance in the model, providing a clear path for understanding the contributions of individual variables to the overall function approximation.

#### D. Learning

KAN and HKAN employ fundamentally different approaches to training, each with distinct characteristics and implications.

KAN utilizes gradient descent in backpropagation process to train the parameters including the weights of the BaFs,  $c$ , and the weights of the spline and SiLU combinations. This approach allows for fine-tuning of the network but introduces the challenges associated with iterative gradient-based optimization, such as potential convergence to local optima and sensitivity to initial conditions.

TABLE II: Comparison of KAN and HKAN.

<b>Basis functions <math>g</math></b>	KAN: B-splines (order 3) HKAN: Flexible (e.g., Gaussian, sigmoid)
<b>Basis function distribution</b>	KAN: Even HKAN: Data-driven or random
<b>Block functions <math>\phi</math></b>	KAN: Weighted sum of spline (linear combination of BaFs) and SiLU HKAN: Linear combination of BaFs
<b>Block function combination <math>h</math></b>	KAN: Added without weights HKAN: Linear combination with weights
<b>Training</b>	KAN: Iterative using backpropagation (gradient descent) HKAN: Non-iterative and hierarchical using least-squares method
<b>Explainability</b>	KAN: BIFs can represent interpretable component functions HKAN: Importance of inputs can be evaluated based on BIFs

HKAN, on the other hand, determines all parameters, i.e. the weights of all linear regressions combining BaFs and blocks, using the least-squares method. The training process is non-iterative and hierarchical, progressing along the network structure. Each layer's weights are determined based on the target function predictions made by the preceding linear regressions, which combine either basis functions or blocks from the previous layer. Only the weights  $c$  of the first-layer blocks are directly determined using input data  $x$ , while subsequent linear regressions successively refine the fitted function to better approximate the target.

The deterministic and non-iterative nature of HKAN's training allows for straightforward estimation of computational complexity (see Section III-D). For KAN, such estimation is challenging due to the unpredictable number of iterations required in the stochastic training process.

HKAN's layer-wise training potentially offers better scalability for deep architectures, as each layer can be optimized independently. KAN's end-to-end training might face challenges with very deep networks due to issues like vanishing gradients.

Table II summarizes the key differences between KAN and HKAN, providing a quick reference for comparison.

## V. HKAN AS MULTI-STACKING MODEL

Stacking has emerged as a highly effective approach for enhancing the predictive power of machine learning models [52]. It employs a meta-learning algorithm to optimally combine predictions generated by different learners. By combining multiple diverse weak learners, an ensemble can reduce the overall error.

In the context of HKAN, BIFs serve as the weak learners, while  $h$ -functions act as the meta-learners. BIFs typically offer a rough nonlinear approximation of the target function within one-dimensional subspaces, providing distinct perspectives on the input data.

Key aspects of ensembling involve two main considerations: how to combine learners and how to generate diversity among them. Diverse weak learners capture various patterns and relationships within the data. This broad coverage helps the ensemble generalize better to new, unseen data, reducing overfitting to the training set and improving model robustness.

In our case, linear regression addresses the combination of learners, while diversity is achieved through the modeling of the target function in one-dimensional subspaces and the randomized distribution of BaFs. Diversity is further controlled by the number of BaFs and the smoothing parameter.

HKAN builds upon BIFs through a stacking approach. The BIFs, each constructed on different projections of individual inputs, are linearly combined to approximate the target function. This combination is performed by multiple stacking  $h$ -functions. Each stacking function integrates a unique set of BIFs, enabling diverse multivariate representations of the target function.

The process extends hierarchically, with the stacking functions from one layer serving as inputs to the next. In each subsequent layer, these stacking functions are nonlinearly transformed by BaFs and then linearly combined to generate new BIFs. These new BIFs are subsequently aggregated to form the stacking functions of the next layer, resulting in a cascade of increasingly complex and abstract representations. Notably, each layer consists of multiple stacking functions ( $h$ ), enabling a parallelized process within each level. This multi-level, parallel stacking architecture allows HKAN to efficiently capture intricate relationships in the data, leveraging the strengths of stacking across multiple scales simultaneously.

## VI. EXPERIMENTAL STUDY

In this section, we compare our proposed HKAN with the standard KAN in regression tasks, evaluating their approximation accuracy. The experimental evaluation was performed on a variety of datasets to validate the model's performance across different regression and function approximation scenarios.

### A. Datasets

The selected datasets include benchmark regression datasets and synthetically generated data designed to emulate complex target functions. They were chosen to evaluate model's ability to generalize across both simple and highly nonlinear relationships.

The synthetic target functions were defined as follows:

$$\begin{aligned}
 \text{TF1: } g(\mathbf{x}) &= (2x_1 - 1)(2x_2 - 1), x_1, x_2 \in [0, 1] \\
 \text{TF2: } g(\mathbf{x}) &= \sum_{i=1}^2 \sin(20 \exp x_i) x_i^2, x_i \in [0, 1] \\
 \text{TF3: } g(\mathbf{x}) &= -\sum_{i=1}^n x_i \sin(\sqrt{|x_i|}), x_i \in [-500, 500] \\
 \text{TF4: } g(\mathbf{x}) &= 1 - \cos\left(2\pi\sqrt{\sum_{i=1}^n x_i^2}\right) - 0.1\sqrt{\sum_{i=1}^n x_i^2}, n = 10, x_i \in [-4, 4] \\
 \text{TF5: } g(\mathbf{x}) &= -\sum_{i=1}^n \sin(x_i) \sin^{20}\left(\frac{ix_i}{\pi}\right), n = 2, 5, x_i \in [0, \pi]
 \end{aligned}$$

Fig. 3 illustrates these functions, each showcasing distinct characteristics. TF1 is a simple saddle-shaped function. TF2 is a complex oscillatory function that combines flat regions with strongly fluctuating ones. TF3 is a periodic wave function with consistent oscillations, exhibiting the highest amplitude near the domain borders. TF4 is a periodic function with radial symmetry. TF5 expresses plateau regions separated by perpendicular grooves of varying depths, with peaks at their intersections.

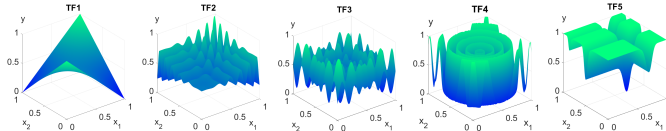


Fig. 3: Synthetic TFs.

TABLE III: Hyperparameter search space for HKAN.

Hyperparameter	Search space
#layers, $L$	{1, 2, 3}
#nodes, $n^{(l)}$	{2, ..., 1000(200)*}
BaF type	Sigmoid (S), Gaussian (G), ReLU (R), Softplus (S+), Tanh (T), Identity** (I)
Smoothing param., $\sigma^{(l)}$	{1, ..., 50}
#BaFs, $m^{(l)}$	{1, ..., 40}
BaF distribution	Random (R), Data-driven (D), Equally spaced** (E)
Regularization param., $\lambda_{\phi}^{(l)}$	{0, 0.001, 0.01, 0.1, 1, 10}

\*1000 for 1- and 2-layer nets, 200 for 3-layer nets.

\*\*Only for the output layer.

All functions, except TF4, have two input arguments. TF4 has ten arguments, while TF5 is evaluated both as a two-argument function and a five-argument variant (TF5-5). The function values and input arguments of TF3, TF4, and TF5 were normalized to the range [0, 1]. Additionally, the TF2 training data was perturbed by adding noise generated from  $U(-0.2, 0.2)$ .

Table V provides an overview of all datasets used in this study, including six synthetically generated datasets and 18 obtained from various sources, as detailed in the table. For these 18 datasets, both input and output variables were normalized to the range [0, 1]. The table also specifies the number of samples, input dimensions, and the sizes of the training and test sets. All datasets are available in our GitHub repository [51].

### B. Optimization

Table III outlines the search space for HKAN hyperparameters. The tree-structured Parzen estimator algorithm, implemented in the Optuna framework [53], was used to explore this space. A total of 1000 trials were conducted, with early stopping applied by pruning trials where the RMSE exceeded twice the baseline RMSE, calculated as the RMSE of the mean prediction on the training set. The optimal hyperparameters were determined using 5-fold cross-validation. The selected hyperparameter values are summarized in Table IV.

KAN optimization was performed using Optuna's trial system, integrated with a grid search sampler [53]. The network's architecture was optimized across a predefined set of configurations:  $\mathcal{W} = \{[n, 1], [n, 2, 1], [n, n + 1, 1], [n, 2n + 1, 1], [n, 2, 2, 1], [n, n + 1, 2, 1], [n, 2n + 1, 2, 1], [n, n + 1, n + 1, 1], [n, 2n + 1, n + 1, 1], [n, 2n + 1, 2n + 1, 1]\}$ . These architectures were chosen based on the original authors' recommendations, emphasizing model accuracy over interpretability.

Initial experiments highlighted the importance of identifying the optimal number of training steps to maximize the performance of the KAN model, as excessive training can lead to overfitting. To mitigate this risk, a 5-fold cross-validation

TABLE IV: Hyperparameters selected for HKAN.

Data	$L$	$n^*$	BaF type**	$\sigma$	$m$	BaF distr.	$\lambda$
TF1	2	932	S, T	1, 33	2, 13	D, D	0.1, 10
TF2	3	48, 11	T, S+, I	22, 18	17, 21	R, D	0.1, 1
TF3	2	924	T, I	50	39	R	.001
TF4	1		T	3	2	E	0.001
TF5	2	912	T, I	50	23	R	0.01
TF5-5	2	1000	T, I	30	32	R	0.001
Abal.	1		I				
Auto.	1		S	9	32	E	0.001
Bank.	1		I				
Comp.	3	189, 30	T, S, R	4, 3, 44	2, 38, 9	D, D, R	10, 1, 0.01
Conc.	3	153, 23	S, S, S	32, 3, 19	10, 2, 11	D, R, D	0.01, 1, 0.01
Dee	1		S	2	38	D	0.1
Ele2	2	478	R, I	19	39	D	0.01
Elev.	2	926	R, S	22, 6	1, 11	D, R	0.001, 0.1
Kin8	3	200, 171	G, S, R	1, 5, 27	4, 3, 30	D, R, R	1, 0.01, 1
Kin32	1		S+	1	40	E	0.001
Laser	2	86	S, S+	23, 15	1, 35	D, D	1, 10
Mach.	1		R	1	25	E	1
Puma.	2	628	G, S+	2, 1	1, 12	D, D	0.001, 0.001
Pyra.	2	678	G, T	48, 33	2, 20	R, D	10, 10
Stock	3	197, 72	S, S+, S	15, 37, 42	1, 3, 24	R, D, R	0.001, 0.001, 0.1
Treas.	2	97	S+, I	3	35	D	1
Triaz.	2	2	S, G	40, 41	29, 6	R, D	1, 0.01
Wiz.	1		I				

\*For the final layer,  $n^{(L)} = 1$  (not shown).

\*\*The identity function (I) does not require any parameters ( $\sigma$ ,  $m$ ,  $\lambda_{\phi}$ , and BaF distribution).

approach was employed to determine the ideal number of training steps at each grid resolution level within a multi-resolution framework. This process was guided by a stopping criterion that halts training when further grid refinement no longer improves model performance.

In summary, the KAN hyperparameter optimization process involved the following steps:

- 1) Iteratively identifying the optimal number of training steps for each grid resolution for every KAN architecture in  $\mathcal{W}$ .
- 2) Evaluating model performance through cross-validation using these optimal training steps.
- 3) Selecting the architecture with the best cross-validation performance.

### C. Results

Table V summarizes the performance metrics for KAN and HKAN, including the median and interquartile range (IQR) of RMSE for both training and test data, calculated from 50 independent training sessions per model. These results are further illustrated in Fig. 4 using boxplots.

The test errors of both models were compared using the Wilcoxon signed-rank test. As shown in Table V, HKAN achieved significantly lower errors than KAN in 12 out of 24 cases, while KAN outperformed HKAN in 9 cases. Notably, HKAN demonstrated superior accuracy on synthetic functions TF1, TF3, TF5, and TF5-5, where its accuracy exceeded that of KAN by several orders of magnitude. For TF2 (a synthetic function with noise), HKAN's errors were over 19% lower than KAN's. A substantial improvement was also observed for the MachineCPU dataset, where HKAN outperformed KAN with a difference exceeding 51%.

Conversely, the largest differences favoring KAN were observed for the Kinematics8nm dataset (over 118%), Ele2 (over 37%), Pumadyn32nh (over 18%), and Elevators (over

TABLE V: Performance comparison of KAN and HKAN.

Data	#samples (training/test) / #arguments	KAN				HKAN			
		Training		Test		Training		Test	
		Median	IQR	Median	IQR	Median	IQR	Median	IQR
TF1	15000 (5000/10000) / 2	5.15E-06	5.59E-06	1.09E-05	1.27E-05	2.68E-14	9.62E-15	<b>3.94E-14</b>	2.00E-14
TF2	15000 (5000/10000) / 2	1.17E-01	4.82E-03	<u>2.29E-02</u>	2.21E-02	1.16E-01	2.21E-04	<b>1.85E-02</b>	1.64E-03
TF3	15000 (5000/10000) / 2	1.14E-02	6.00E-03	1.22E-02	7.58E-03	6.37E-06	5.88E-08	<b>5.08E-06</b>	3.85E-07
TF4	5000 (3750/1250) / 10	2.58E-01	4.50E-06	2.59E-01	5.42E-05	2.60E-01	0	<b>2.58E-01</b>	0
TF5	15000 (5000/10000) / 2	3.31E-05	3.26E-05	8.58E-05	1.06E-04	2.98E-15	4.58E-16	<b>4.56E-15</b>	2.39E-15
TF5-5	10000 (7500/2500) / 5	3.83E-03	4.12E-03	5.07E-03	5.51E-03	3.40E-09	8.70E-10	<b>3.93E-09</b>	9.88E-10
Abalone [54]	4177 (313/1044) / 8	7.26E-02	6.00E-04	<b>7.52E-02</b>	1.00E-03	7.80E-02	0	8.00E-02	0
AutoMPG [54]	386 (270/116) / 7	5.31E-02	2.78E-03	<b>8.04E-02</b>	4.85E-03	6.80E-02	0	8.38E-02	0
Bank32nh [55]	8192 (5734/2458) / 32	9.54E-02	1.81E-03	<b>9.87E-02</b>	1.50E-03	1.02E-01	0	<u>1.01E-01</u>	0
Compactive [56]	8192 (6144/2048) / 21	2.27E-02	4.61E-04	2.47E-02	1.34E-03	2.24E-02	1.19E-04	<b>2.37E-02</b>	3.94E-04
Concrete [54]	1030 (773/257) / 8	5.23E-02	2.55E-03	6.48E-02	3.33E-03	4.67E-02	1.26E-03	<b>6.12E-02</b>	2.30E-03
Dee [56]	365 (274/91) / 6	7.15E-02	3.29E-03	1.05E-01	4.85E-03	8.63E-02	1.10E-04	<b>1.03E-01</b>	1.22E-04
Ele2 [56]	1056 (792/264) / 4	6.44E-03	7.37E-04	<b>7.33E-03</b>	6.07E-04	7.88E-03	4.78E-07	1.01E-02	9.85E-07
Elevators [56]	16599 (11619/4980) / 18	2.74E-02	4.37E-04	<b>2.95E-02</b>	5.62E-04	2.85E-02	1.73E-04	3.35E-02	6.34E-04
Kinematics8nm [55]	8192 (6144/2048) / 8	3.94E-02	4.77E-04	<b>4.63E-02</b>	1.57E-03	9.55E-02	1.15E-03	1.01E-01	1.09E-03
Kinematics32nh [55]	8192 (5734/2458) / 32	1.21E-01	6.38E-03	<b>1.32E-01</b>	4.44E-03	1.33E-01	0	1.35E-01	0
Laser [56]	993 (745/248) / 4	1.44E-02	5.78E-04	2.35E-02	1.41E-02	1.46E-02	7.41E-04	2.56E-02	3.62E-03
MachineCPU [56]	209 (146/63) / 6	1.76E-02	6.03E-04	8.54E-02	4.66E-02	4.13E-02	0	<b>4.13E-02</b>	0
Pumadyn32nh [55]	8192 (5734/2458) / 32	2.69E-02	1.95E-03	<b>3.90E-02</b>	1.93E-03	4.19E-02	2.08E-04	4.61E-02	6.03E-04
Pyramidines [57]	74 (52/22) / 27	3.08E-02	5.72E-03	1.03E-01	2.50E-02	7.34E-16	1.40E-16	9.89E-02	1.93E-02
Stock [56]	950 (713/237) / 9	2.06E-02	1.14E-03	2.83E-02	1.55E-03	1.63E-02	4.77E-04	2.81E-02	1.75E-03
Treasury [56]	1049 (734/315) / 15	8.69E-03	3.99E-04	1.18E-02	1.50E-03	9.49E-03	6.41E-05	<b>1.11E-02</b>	1.56E-04
Triazines [57]	186 (130/56) / 60	1.37E-01	1.37E-02	<b>1.83E-01</b>	1.88E-02	1.83E-01	1.14E-02	1.98E-01	7.51E-03
Wizmir [56]	1461 (1096/365) / 9	1.65E-02	3.60E-04	2.01E-02	2.75E-03	2.10E-02	0	<b>1.97E-02</b>	0

The test errors of both models were compared using the Wilcoxon test, with significantly lower values highlighted in **bold**.

The test and training errors were compared separately for each model using the Wilcoxon test, with significantly lower test errors underlined.

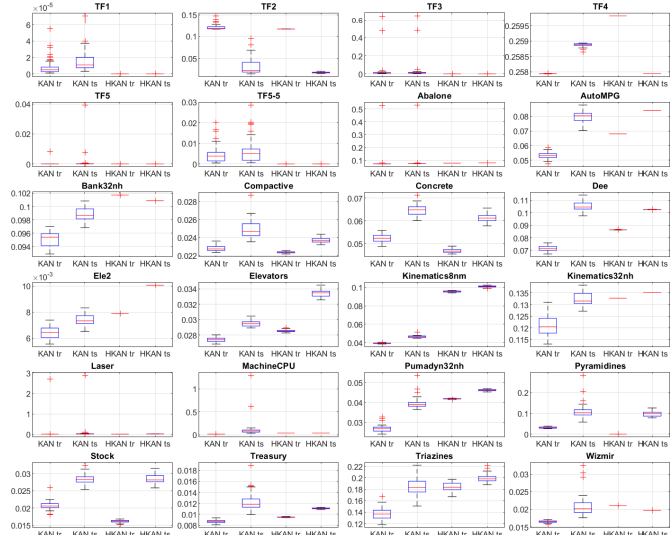


Fig. 4: Distribution of training (tr) and test (ts) RMSE for KAN and HKAN.

13%). For the remaining datasets, the differences in test errors between the two models were within 10%.

When comparing training and test errors for each model separately, it was observed that, in most cases, the training error was significantly lower than the test error, as confirmed by the Wilcoxon test. Cases where the test error was significantly lower than the training error were rare, occurring five times for HKAN and only once for KAN (see the underlined errors in Table V). Substantially lower training errors compared to test errors may indicate overfitting, differences in the distributions of training and test sets, insufficient representation of the test

set in the training data, or an inadequate number of training samples relative to the number of input arguments.

The IQR serves as a measure of model variance, reflecting the consistency of predictions across different training sessions. As shown in Table V and Fig. 4, HKAN produces more stable results than KAN in all cases except for the Elevators and Stock datasets. HKAN frequently exhibits an IQR of 0, indicating deterministic behavior. This occurs when the optimal architecture comprises a single layer ( $L = 1$ ) with identity BaFs or uniformly spaced BaFs (refer to Table IV for the optimal hyperparameters). Under such conditions, HKAN consistently produces identical results across all training sessions.

#### D. How HKAN Constructs Fitted Function

This section analyzes how HKAN constructs a fitted function layer by layer. Fig. 5 provides an example for TF2. The two upper panels illustrate the functions fitted at successive levels of HKAN processing (successive linear regressions), specifically the BIFs of the first layer ( $\phi^{(1)}$ ), the  $h$ -functions of the first layer ( $h^{(1)}$ ), the BIFs of the second layer ( $\phi^{(2)}$ ), the  $h$ -functions of the second layer ( $h^{(2)}$ ), the BIFs of the third layer ( $\phi^{(3)}$ ), and the  $h$ -function of the third layer ( $h^{(3)}$ ).

At each level, except the final one, multiple functions are fitted in parallel; for clarity, only two representative functions are displayed in the two upper panels. The lower panel presents predicted vs. target plots for five selected fitted functions at each processing level, excluding the final level, where only a single function is created.

The following insights can be drawn from Fig. 5:

- 1) Shapes and Complexity of the Fitted Functions: The fitted function evolves in shape and complexity as it

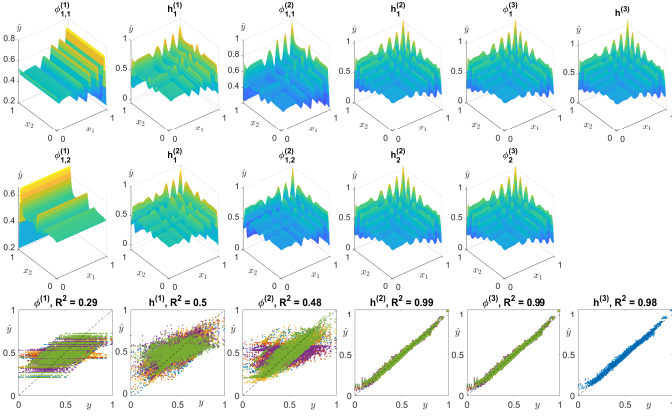


Fig. 5: Fitted functions and predicted vs. target plots at successive levels of HKAN processing for TF2.

progresses through the layers. At the first level, the target function is modeled nonlinearly using individual input variables, capturing only the features apparent in these variables, such as localized fluctuations. The second level integrates these preliminary approximations across all input variables, producing a multi-variable approximation that remains relatively coarse. The subsequent two levels — nonlinear transformations by the blocks of the second layer followed by linear combinations of their outputs — significantly improve the approximation quality. The fifth and sixth levels refine the result by processing the fourth-level outputs in a similar manner.

- 2) Modeling Variance: The modeling variance, represented by deviations from the diagonal zero-error line in the predicted vs. target plots, decreases significantly across successive levels. At the first level, the fitted functions display high variance and are constrained to a narrow range of approximately 0.2-0.75. In subsequent levels, the range progressively expands. By the forth level, the modeling variance is significantly reduced, and the range widens to its full extent. However, small deviations from the diagonal persist at the boundaries, indicating that the extreme values of the target function are not fully captured by the HKAN model.
- 3) Diversity in Blocks and Nodes: Each block produces a distinct BIF due to differing inputs and the distribution of BaFs. Significant diversity is observed among the BIFs in the first and second layers, as well as among the nodes in the first layer. However, this diversity diminishes at the second layer's output, where individual nodes achieve a more accurate approximation of the target function. In the third layer, diversity among BIFs is limited, as blocks in this layer process more uniform inputs.

Figs. 6 and 7 illustrate examples of HKAN's fitting for TF3 and TF5. Unlike TF2, these target functions were not affected by noise, enabling HKAN to achieve nearly perfect fitting with just two layers.

Additional examples are presented in Fig. 8. Among these, the Concrete dataset required the most complex architecture

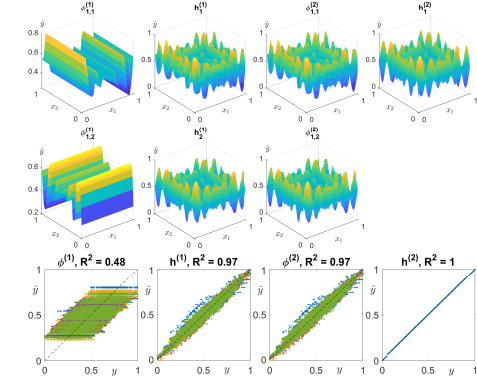


Fig. 6: Fitted functions and predicted vs. target plots at successive levels of HKAN processing for TF3.

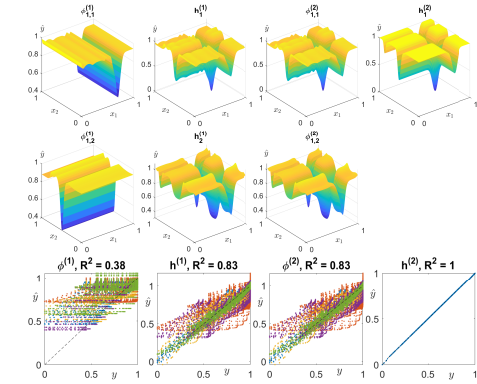


Fig. 7: Fitted functions and predicted vs. target plots at successive levels of HKAN processing for TF5.

with three layers, while the Abalone dataset achieved its best fit with a simple architecture of just one layer. However, the latter case demonstrates that satisfactory results are not always guaranteed.

These visualizations emphasize HKAN's hierarchical modeling process, where prediction quality is progressively refined through successive layers, adapting to the complexity and structure of the target function.

#### E. Input Argument Importance Estimation by HKAN

HKAN includes a built-in mechanism for estimating the importance of input arguments. The blocks in the first layer approximate the target function based on individual inputs, and the accuracy of each block's fitting, measured by  $R^2$ , serves as a proxy for the importance of the corresponding input. However, it should be noted that this importance is estimated based on the coarse approximation performed by the first-layer blocks. The more refined approximations developed in subsequent layers are not considered in this estimation.

Fig. 9 presents boxplots of the  $R^2$  values for predictions made by the first-layer blocks. In some cases, such as TF1 and TF4, all  $R^2$  values are very small (less than 0.01), indicating that the blocks provide a very weak approximation of the target function. By contrast, significantly higher  $R^2$  values observed for other synthetic functions highlight a more

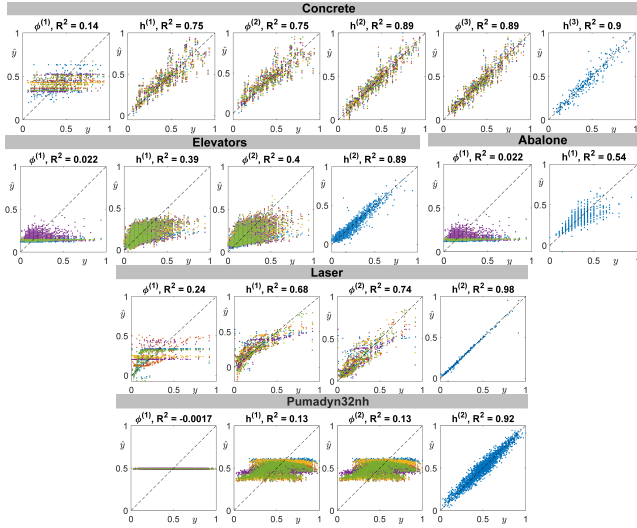
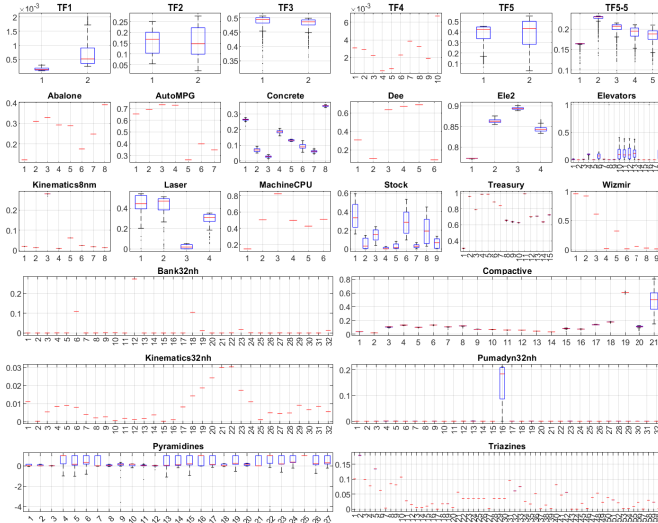


Fig. 8: Predicted vs. target plots for selected datasets.

Fig. 9: Input arguments importance:  $R^2$  for first-layer BIFs.

balanced importance across input arguments, which aligns with expectations.

The greatest variation in  $R^2$  values among input variables, exceeding 0.5, is observed for datasets such as Compactive, Dee, MachineCPU, Pyramidines, Stock, Treasury, and Wizmir. In these cases, large differences in variable importance are evident even during the coarse modeling of the target function by the first-layer blocks.

The average importance of the  $p$ -th input argument can be estimated using the BIFs associated with this argument as their average  $R^2$ :

$$I_p = \frac{1}{n^{(1)}} \sum_{q=1}^{n^{(1)}} R^2(y, \phi_{q,p}^{(1)}) \quad (14)$$

## F. Discussion

The experimental results highlight HKAN's potential as a robust alternative to backpropagation-based KAN. Its hi-

erarchical multi-stacking approach and randomized learning process make it particularly well-suited for applications that require rapid model deployment and transparency in variable importance.

HKAN eliminates the iterative backpropagation process, significantly reducing computational complexity. By transforming the optimization problem into multiple convex subproblems solved using least-squares regression, HKAN ensures efficient training while maintaining accuracy. Its deterministic training process enhances stability, while the layer-by-layer hierarchical approach facilitates transparent function representation. The flexibility of HKAN's architecture offers a notable advantage in capturing diverse functional relationships within the data.

In HKAN, the fitted functions are constructed hierarchically, evolving in shape and complexity across layers. An initial layer focuses on features derived from individual input variables, while subsequent layers integrate these approximations across all variables and progressively refine their quality. As the network deepens, modeling variance decreases significantly, contributing to the accuracy and stability of the model's predictions.

HKAN incorporates two ensemble-like principles that enhance its generalization and robustness:

- 1) Horizontal Integration: Within each layer, diverse blocks are combined, akin to ensemble methods. Each block offers a unique perspective on the input data, and their aggregation enables the network to capture a broader range of patterns and relationships.
- 2) Vertical Integration: The layer-by-layer processing corresponds to multi-level stacking, where each successive layer builds on the approximations learned by the previous one. This approach allows the network to construct increasingly complex functions.

These ensemble-like properties enable HKAN to model intricate relationships in the data without relying on backpropagation, offering a distinctive approach to function approximation and pattern recognition tasks.

A key strength of HKAN is its built-in mechanism for estimating the importance of input arguments, providing valuable insights into the significance of individual variables. This feature enhances interpretability, making HKAN particularly useful in applications where understanding variable contributions is crucial. In contrast, the interpretability of KAN stems from its ability to explicitly model functional relationships between input arguments and the output variable, enabling an understanding of both the nature and extent of each input's influence on predictions.

The complexity of the target function directly influences the optimal architecture of HKAN. More complex target functions require deeper and wider networks, while simpler functions can be effectively modeled with fewer layers, blocks, and BaFs. HKAN's flexibility in selecting BaFs further sets it apart. While KAN relies on B-splines, which can be computationally intensive due to recursive processing, HKAN supports alternative BaFs such as Gaussian and sigmoid, among others. Furthermore, HKAN allows for data-driven or random distributions of BaFs, whereas KAN typically employs

evenly distributed BaFs. The smoothing parameter in HKAN is another critical hyperparameter, providing additional control over the model's adaptability.

## VII. CONCLUSION

This study introduces the Hierarchical Kolmogorov-Arnold Network as an efficient and interpretable alternative to traditional backpropagation-based NNs, particularly KAN. By employing a randomized learning approach based on linear regression and a hierarchical multi-stacking architecture, HKAN eliminates the need for iterative gradient-based training, reducing computational complexity while maintaining or even enhancing accuracy and stability.

The empirical evaluation demonstrates that HKAN performs competitively across diverse regression tasks, effectively capturing complex relationships within data. Additionally, its built-in mechanism for estimating input variable importance enhances interpretability, making it a valuable tool for applications requiring transparency and explainability. The flexibility of HKAN in terms of basis functions and architecture allows it to adapt to varying complexities of target functions, further establishing its potential for real-world applications.

Future research could explore extending HKAN's capabilities to classification and forecasting tasks, as well as investigating its integration with other advanced architectures to expand its applicability.

## REFERENCES

- [1] Z. Liu et al., "KAN: Kolmogorov-Arnold Networks," arXiv preprint arXiv:2404.19756, 2024.
- [2] M. E. Samadi, Y. Müller, and A. Schuppert, "Smooth Kolmogorov Arnold networks enabling structural knowledge representation," arXiv preprint arXiv:2405.11318, 2024.
- [3] Y. Peng et al., "Predictive modeling of flexible EHD pumps using Kolmogorov-Arnold Networks," *Biomimetic Intelligence and Robotics*, vol. 4, no. 4, pp. 100184, 2024.
- [4] K. Shukla, J. D. Toscano, Z. Wang, Z. Zou, and G. E. Karniadakis, "A comprehensive and fair comparison between MLP and KAN representations for differential equations and operator networks," arXiv preprint arXiv:2406.02917, 2024.
- [5] S.S. Sidharth, R. Gokul, K.P. Anas, and A.R. Keerthana, "Chebyshev polynomial-based Kolmogorov-Arnold networks: An efficient architecture for nonlinear function approximation," arXiv preprint arXiv:2405.07200, 2024.
- [6] Y. Wang, J. W. Siegel, Z. Liu, and T. Y. Hou, "On the expressiveness and spectral bias of KANs," arXiv preprint arXiv:2410.01803, 2024.
- [7] J.-D. Park, K.-M. Kim, and W.-Y. Shin, "CF-KAN: Kolmogorov-Arnold network-based collaborative filtering to mitigate catastrophic forgetting in recommender systems," arXiv preprint arXiv:2409.05878, 2024.
- [8] R. Yu, W. Yu, and X. Wang, "KAN or MLP: A fairer comparison," arXiv preprint arXiv:2407.16674, 2024.
- [9] V. D. Tran et al., "Exploring the limitations of Kolmogorov-Arnold networks in classification: Insights to software training and hardware implementation," arXiv preprint arXiv:2407.17790, 2024.
- [10] H. Shen, C. Zeng, J. Wang, and Q. Wang, "Reduced effectiveness of Kolmogorov-Arnold networks on functions with noise," arXiv preprint arXiv:2407.14882, 2024.
- [11] Z. Liu, P. Ma, Y. Wang, W. Matusik, and M. Tegmark, "KAN 2.0: Kolmogorov-Arnold networks meet science," arXiv preprint arXiv:2408.10205, 2024.
- [12] A. D. Bodner, A. S. Tepsich, J. N. Spolski, and S. Pourteau, "Convolutional Kolmogorov-Arnold networks," arXiv preprint arXiv:2406.13155, 2024.
- [13] R. C. Yu, S. Wu, and J. Gui, "Residual Kolmogorov-Arnold network for enhanced deep learning," arXiv preprint arXiv:2410.05500, 2024.
- [14] R. Genet and H. Inzirillo, "A temporal Kolmogorov-Arnold transformer for time series forecasting," arXiv preprint arXiv:2406.02486, 2024.
- [15] R. Genet and H. Inzirillo, "TKAN: Temporal Kolmogorov-Arnold networks," arXiv preprint arXiv:2405.07344, 2024.
- [16] H. Inzirillo and R. Genet, "SigKAN: Signature-weighted Kolmogorov-Arnold networks for time series," arXiv preprint arXiv:2406.17890, 2024.
- [17] X. Yang and X. Wang, "Kolmogorov-Arnold transformer," arXiv preprint arXiv:2409.10594, 2024.
- [18] F. Zhang and X. Zhang, "GraphKAN: Enhancing feature extraction with graph Kolmogorov-Arnold networks," arXiv preprint arXiv:2406.13597, 2024.
- [19] R. Li, M. Li, W. Liu, and H. Chen, "GNN-SKAN: Harnessing the power of SwallowKAN to advance molecular representation learning with GNNs," arXiv preprint arXiv:2408.01018, 2024.
- [20] H. Hao, X. Zhang, B. Li, and A. Zhou, "A first look at Kolmogorov-Arnold networks in surrogate-assisted evolutionary algorithms," arXiv preprint arXiv:2405.16494, 2024.
- [21] A. S. Chen, "Gaussian process Kolmogorov-Arnold networks," arXiv preprint arXiv:2407.18397, 2024.
- [22] Z. Bozorgasl and H. Chen, "Wav-KAN: Wavelet Kolmogorov-Arnold networks," arXiv preprint arXiv:2405.12832, 2024.
- [23] D. W. Abueidda, P. Pantidis, and M. E. Mobasher, "DeepOKAN: Deep Operator Network based on Kolmogorov Arnold networks for mechanics problems," arXiv preprint arXiv:2405.19143, 2024.
- [24] J. Xu, Z. Chen, J. Li, S. Yang, W. Wang, X. Hu, and E. C.-H. Ngai, "FourierKAN-GCF: Fourier Kolmogorov-Arnold Network – An effective and efficient feature transformation for graph collaborative filtering," arXiv preprint arXiv:2406.01034, 2024.
- [25] A. A. Aghaei, "FKAN: Fractional Kolmogorov-Arnold networks with trainable Jacobi basis functions," arXiv preprint arXiv:2406.07456, 2024.
- [26] A. A. Aghaei, "RKAN: Rational Kolmogorov-Arnold networks," arXiv preprint arXiv:2406.14495, 2024.
- [27] Q. Qiu, T. Zhu, H. Gong, L. Chen, and H. Ning, "ReLU-KAN: New Kolmogorov-Arnold networks that only need matrix addition, dot multiplication, and ReLU," arXiv preprint arXiv:2406.02075, 2024.
- [28] H.-T. Ta, D.-Q. Thai, A. B. S. Rahman, G. Sidorov, and A. Gelbukh, "FC-KAN: Function combinations in Kolmogorov-Arnold networks," arXiv preprint arXiv:2409.01763, 2024.
- [29] M. G. Altarabichi, "DropKAN: Regularizing KANs by masking post-activations," arXiv preprint arXiv:2407.13044, 2024.
- [30] S. Rigas, M. Papachristou, T. Papadopoulos, F. Anagnostopoulos, and G. Alexandridis, "Adaptive training of grid-dependent physics-informed Kolmogorov-Arnold networks," arXiv preprint arXiv:2407.17611, 2024.
- [31] E. Zeydan, C. J. Vaca-Rubio, L. Blanco, R. Pereira, M. Caus, and A. Aydeger, "F-KANs: Federated Kolmogorov-Arnold networks," arXiv preprint arXiv:2407.20100, 2024.
- [32] V. A. Kich, J. A. Bottega, R. Steinmetz, R. B. Grando, A. Yorozu, and A. Ohya, "Kolmogorov-Arnold Network for Online Reinforcement Learning," arXiv preprint arXiv:2408.04841, 2024.
- [33] E. Poeta, F. Giobergia, E. Pastor, T. Cerquitelli, and E. Baralis, "A benchmarking study of Kolmogorov-Arnold networks on tabular data," arXiv preprint arXiv:2406.14529, 2024.
- [34] C. Li, X. Liu, W. Li, C. Wang, H. Liu, and Y. Yuan, "U-KAN makes strong backbone for medical image segmentation and generation," arXiv preprint arXiv:2406.02918, 2024.
- [35] C. J. Vaca-Rubio, L. Blanco, R. Pereira, and M. Caus, "Kolmogorov-Arnold networks (KANs) for time series analysis," arXiv preprint arXiv:2405.08790, 2024.
- [36] K. Xu, L. Chen, and S. Wang, "Kolmogorov-Arnold networks for time series: Bridging predictive power and interpretability," arXiv preprint arXiv:2406.02496, 2024.
- [37] Q. Zhou et al., "KAN-AD: Time series anomaly detection with Kolmogorov-Arnold networks," arXiv preprint arXiv:2411.00278, 2024.
- [38] S. Yang, L. Qin, and X. Yu, "Endowing interpretability for neural cognitive diagnosis by efficient Kolmogorov-Arnold networks," arXiv preprint arXiv:2405.14399, 2024.
- [39] A. Kundu, A. Sarkar, and A. Sadhu, "KANQAS: Kolmogorov-Arnold network for quantum architecture search," arXiv preprint arXiv:2406.17630, 2024.
- [40] P. Pratyush, C. Carrier, S. Pokharel, H. D. Ismail, M. Chaudhari, and D. B. KC, "CaLMPHosKAN: Prediction of general phosphorylation sites in proteins via fusion of codon aware embeddings with amino acid aware embeddings and wavelet-based Kolmogorov-Arnold network," bioRxiv preprint, <https://doi.org/10.1101/2024.07.30.605530>, 2024.
- [41] W. Knottenbelt, Z. Gao, R. Wray, W. Z. Zhang, J. Liu, and M. Crispin-Ortuzar, "CoxKAN: Kolmogorov-Arnold networks for interpretable, high-performance survival analysis," arXiv preprint arXiv:2409.04290, 2024.

- [42] J. Principe and B. Chen, "Universal approximation with convex optimization: Gimmick or reality?" *IEEE Comput. Intell. Mag.*, vol. 10, no. 2, pp. 68–77, 2015.
- [43] Y. Pao, G. Park, and D. Sobejic, "Learning and generalization characteristics of the Random Vector Functional-Link net," *Neurocomputing*, vol. 6, no. 2, pp. 163–180, 1994.
- [44] D. Needell, A.A. Nelson, R. Saab, P. Salanevich, and O. Schavemaker, "Random Vector Functional Link networks for function approximation on manifolds," *Front. Appl. Math. Stat.*, vol. 10, 2024.
- [45] L. Zhang and P. Suganthan, "A comprehensive evaluation of Random Vector Functional Link networks," *Inform. Sci.*, vols. 367–368, pp. 1094–1105, 2016.
- [46] S. Scardapane and D. Wang, "Randomness in neural networks: An overview," *WIREs Data Mining and Knowledge Discovery*, vol. 7, no. 2, pp. e1200, 2017.
- [47] A. K. Malik, R. Gao, M. A. Ganaie, M. Tanveer, and P. N. Suganthan, "Random Vector Functional Link network: Recent developments, applications, and future directions," *Applied Soft Computing*, vol. 143, pp. 110377, 2023.
- [48] G. Dudek, "Generating random weights and biases in feedforward neural networks with random hidden nodes," *Information Sciences*, vol. 481, pp. 33–56, 2019.
- [49] G. Dudek, "Generating random parameters in feedforward neural networks with random hidden nodes: Drawbacks of the standard method and how to improve it," In *Proc. Neural Information Processing, ICONIP 2020, Communications in Computer and Information Science*, vol. 1333, pp. 598–606, 2020.
- [50] G. Dudek, "A constructive approach to data-driven randomized learning for feedforward neural networks," *Applied Soft Computing*, vol. 112, pp. 107797, 2021.
- [51] T. Rodak, "HKAN: Hierarchical Kolmogorov-Arnold network without backpropagation - code and data," <https://github.com/rodakt/hkan>, 2025.
- [52] D. H. Wolpert, "Stacked generalization," *Neural Networks*, vol. 5, no. 2, pp. 241–259, 1992.
- [53] T. Akiba, S. Sano, T. Yanase, T. Ohta, and M. Koyama, "Optuna: A Next-generation hyperparameter optimization framework," in *Proceedings of the 25th ACM SIGKDD International Conference on Knowledge Discovery and Data Mining*, 2019.
- [54] K. Bache and M. Lichman, "UCI machine learning repository," 2017 (Accessed 22 July 2016).
- [55] "Data for Evaluating Learning in Valid Experiments (DELVE Project)," <https://www.cs.toronto.edu/~delve/data/datasets.html>, (Accessed 22 July 2016).
- [56] J. Alcalá-Fdez, A. Fernandez, J. Luengo, J. Derrac, S. García, L. Sánchez, and F. Herrera, "KEEL data-mining software tool: data set repository, integration of algorithms and experimental analysis framework," *Journal of Multiple-Valued Logic and Soft Computing*, vol. 17, no. 2–3, pp. 255–287, 2011.
- [57] L. Torgo, "Regression DataSets," <http://www.dcc.fc.up.pt/~ltorgo/Regression/DataSets> (Accessed 2 July 2016).